Pakistan Veterinary Journal

ISSN: 0253-8318 (PRINT), 2074-7764 (ONLINE)
DOI: 10.29261/pakvetj/2025.217

RESEARCH ARTICLE

Toxicological Assessment of Iron Oxide Nanoparticles: Hematological and Hepatic Biomarkers in Sprague-Dawley Rats

Mamoona Akhtar[1], Farhat Jabeen[1], Salma Ikram[2], Maria Manan[3], Hina Rizvi[4] and Muhammad Kashif Zahoor[1,*]

[1]Department of Zoology, Government College University Faisalabad, Pakistan; [2]Department of Physics, Government College University Faisalabad, Pakistan; [3]Department of Pharmacology, Government College University Faisalabad, Pakistan; [4]Department of Environmental Sciences and Engineering, Government College University, Faisalabad, Pakistan
*Corresponding author: kashif.zahoor@gcuf.edu.pk

ARTICLE HISTORY (25-527)

Received: June 06, 2025
Revised: July 20, 2025
Accepted: July 21, 2025
Published online: August 11, 2025

Key words:
Hematotoxicity
Hepatotoxicity
Lipid metabolism
Liver damage
Nanoparticles

ABSTRACT

Iron Oxide Nanoparticles are widely used in various industries including medicine, water purification, removal of pollutants and cosmetics. However, certain environmental and human health concerns remain unaddressed even when they may accumulate in soil and water. The current study was devised to examine the hepatotoxic and hematotoxic effects of iron oxide nanoparticles (Fe_2O_3-NPs) in Sprague-Dawley rats. Twenty-five rats weighing 95-118 g were split up into five groups (n=5): control (without any treatment), saline (9% NaCl) and three treatment groups, which received intraperitoneal injections of Fe_2O_3-NPs at low (75 mg/kg), medium (150 mg/kg) and high (300 mg/kg) doses for a duration of 28 days. The body weights of all the rats were recorded every week. It was revealed that the effect of iron oxide nanoparticles was dose-dependent and had a major influence on lipid metabolism and liver function. Higher dosages resulted in increased level of cholesterol, triglycerides and total lipids, which may indicate dyslipidemia and hepatic lipid buildup. While bilirubin levels were constant among groups, elevated levels of ALP, ALT (SGPT) and AST (SGOT) suggested hepatic stress and possible liver damage. WBCs counts dramatically increased at medium and high doses but there were no discernible changes observed in monocytes, eosinophils, neutrophils or lymphocytes. Hemoglobin levels did not alter appreciably. Histopathological analysis of liver showed severe vascular congestion, sinusoidal dilatation and erythrocyte aggregation in a dose-dependent manner. These results affirm the necessity of cautious dose guidelines in biomedical applications and underline the possible hazards of exposure to high doses of iron oxide nanoparticles.

To Cite This Article: Akhtar M, Jabeen F, Ikram S, Manan M, Rizvi H and Zahoor MK 2025. Toxicological assessment of iron oxide nanoparticles: hematological and hepatic biomarkers in sprague-dawley rats. Pak Vet J. http://dx.doi.org/10.29261/pakvetj/2025.217

INTRODUCTION

Nanotoxicology examines the safety issues regarding nanoparticles (NPs), with particular emphasis on how they interact with biological systems (ALRashdi *et al*., 2023; Abd Elaliem *et al*., 2023; Rathore *et al*., 2023; Ahmed *et al*., 2024; Hannan *et al*., 2024; Eid, 2025; Joshi and Awasthi, 2025). Different biological reactions are induced by nanoparticles depending on their size, shape, composition, and surface chemistry. The NPs are divided into two groups: incidental nanoparticles, which are generated accidentally, like diesel particles, and engineered nanoparticles (ENPs), which include carbon nanotubes, dendrimers, fullerenes, and quantum dots with sizes less than 100 nm (Khan *et al*., 2019; Ma *et al*., 2024; Shah *et al*., 2024; Poonia *et al*., 2025; Sing *et al*., 2025). NPs can enter the body through a variety of entry portals, including cutaneous, pulmonary, gastrointestinal, and intravenous systems. The body's barrier and clearance systems, as well as the exposure route, affect how harmful are the NPs (Rana, 2020; Rathore *et al*., 2023; Ahmed *et al*., 2024; Hannan *et al*., 2024). The magnetic nanoparticles are composed of iron, nickel and cobalt; and have special characteristics that enable them manipulated in magnetic fields Magnetic nanoparticles are rapidly absorbed into the bloodstream after being consumed or inhaled, with the liver accounting for 80-90% of

accumulation, followed by spleen (5-8%) and bone marrow (1-2%) (Parivar *et al*., 2016; Ahmed *et al*., 2024).

Magnetite (Fe_3O_4) and maghemite (γ- Fe_2O_3) make up majority of iron oxide nanoparticles (IONPs), a subtype of magnetic nanoparticles with diameters ranging from 1 to 100 nm (Dietrich *et al*., 2023). IONPs offer a wide range of biomedical uses, such as medication delivery, environmental remediation and imaging, because of their magnetic qualities, biocompatibility and simplicity of synthesis (Ali *et al*., 2016; Rathore *et al*., 2023; Ahmed *et al*., 2024). Co-precipitation, thermal breakdown and pyrolysis are examples of physical, biological, or chemical processes that can be used to create IONPs (Khan *et al*., 2019). However, their application for drug delivery raises concerns since they can result in problems like toxicity, non-specific transport and low solubility (Rathore *et al*., 2023). By increasing the permeability of target tissues or employing external magnetic fields, active or passive targeting can lessen these effects (Bică *et al*., 2024).

Nanoparticles have special physicochemical characteristics that make them extremely adaptable for clinical and biological applications because of their small size and high surface-area-to-volume ratio. They are used in regenerative medicine, immunodiagnostics, drug delivery and hyperthermia-based cancer treatment (Parivar *et al*., 2016; Khan *et al*., 2019; Ahmed *et al*., 2024; Panda and Das, 2025; Poonia *et al*., 2025; Szymczuk *et al*., 2025). They are becoming more useful in environmental remediation because of their vast surface area which also helps with bioengineering, biosensing, and water purification (Elahi & Rizwan, 2021; Schneider *et al*., 2022; Ahmed *et al*., 2024).

Although, iron is a transition metal, which is found in large quantities in nature; however, the toxicity of iron oxide nanoparticles is different from that of bulk iron due to their small size and surface reactivity (Khan *et al*., 2019; Aboulhoda *et al*., 2023; Al Alalaq *et al*., 2023). Furthermore, nanoparticles can be more harmful than their bulk counterparts because of their increased capacity for oxidative stress, bioaccumulation, and tissue damage (Reddy *et al*., 2018; Abawy *et al*., 2023; Al Alalaq *et al*., 2023). Iron oxide nanoparticles (Fe_2O_3-NPs), one of the most widely utilized nanoparticles in nanotechnology, have been connected to mitochondrial dysfunction, DNA damage, and oxidative stress (Siddiqui *et al*., 2023; Shah *et al*., 2024; Buck *et al*., 2025). Although, coating iron oxide nanoparticles can enhance their biodistribution, stability and biocompatibility; but the cytotoxicity and oxidative stress are still the issues (Laubertova *et al*., 2022; Benjamin and Nayak, 2025; Regan *et al*., 2025).

In human physiology, iron is essential especially for cellular metabolism and oxygen transport. But too much iron can cause oxidative stress, which ages cells and damages tissue like liver, heart, kidney, brain, nervous system and lungs (Hasabo *et al*., 2015; Gaharwar *et al*., 2019; Siddiqui *et al*., 2023; Innuan *et al*., 2025; Jasim *et al*., 2025). Although magnetic nanoparticles, like superparamagnetic iron oxide nanoparticles (USPIONs), increase the sensitivity of magnetic resonance imaging (MRI), there have been worries expressed over their possible toxicity, particularly after repeated exposure (Dietrich *et al*., 2023; Mirzajani *et al*., 2024; Innuan *et al*., 2025).

Ingestion, inhalation and skin contact are some of the ways that nanoparticles can enter the body. After entering the bloodstream, nanoparticles interact with plasma proteins and immune cells, which may result in oxidative stress, cellular damage and immunological activation (Taher *et al*., 2022; Abd Elaliem *et al*., 2023; Mohamed *et al*., 2024). It has been shown that iron oxide nanoparticles affect oxidative stress and the antioxidant defense system in liver and kidney tissues (Reddy *et al*., 2017; Laubertova *et al*., 2022; Siddiqui *et al*., 2023). By interfering with cellular proteins and enzymatic processes, iron oxide nanoparticles cause oxidative stress, which damages tissue and cause cellular degeneration. Histological alterations in the liver and blood tissues, characterized by cytoplasmic degradation, are indicative of this imbalance in oxidative stress (Gaharwar *et al*., 2019; Abd Elaliem *et al*., 2023; Siddiqui *et al*., 2023).

The enzymatic activity of glutathione peroxidase (GPx) and superoxide dismutase (SOD) as well as malondialdehyde (MDA) levels varied in a dose-dependent manner (Aboulhoda *et al*., 2023). Toxicological symptoms in humans include anaphylactic shock, nausea, vomiting, and chest pain (Kurapov *et al*., 2019; Kamel and AL-Taee., 2020; Abawy *et al*., 2023; Awad *et al*., 2024; Kazaryan *et al*., 2024). Since the liver is the main organ involved in detoxification, it collects the most nanoparticles, which may have dose-dependent consequences such as tissue damage, inflammation, and oxidative stress (Parivar *et al*., 2016; Abawy *et al*., 2023; Kazaryan *et al*., 2024). Long-term exposure to IONPs may also upset the gut-liver axis and worsen liver diseases such nonalcoholic fatty liver disease (NAFLD) (Rana 2020; Shokrollahi *et al*., 2023; Al Alalaq *et al*., 2023).

Iron oxide nanoparticles have also demonstrated potential in blood-related applications like drug delivery and imaging (Ahmed *et al*., 2024; Rathore *et al*., 2023). IONPs can cause complement activation and inflammation, which could hinder their clinical application, therefore their interactions with blood components need to be carefully watched (Zhang *et al*., 2024; Liu *et al*., 2025). IONPs have many prospective uses, especially in targeted medication administration and imaging, but little is known about the possible health concerns associated with them (Khan *et al*., 2019; Ahmed *et al*., 2024; Sing *et al*., 2025). IONPs are a promising choice for medical applications due to their biocompatibility, physical and chemical characteristics, and ease of synthesis (Ahmed *et al*., 2024; Sing *et al*., 2025).

Despite being widely used worldwide in medical and biological applications as targeted drug administration and magnetic resonance imaging, because of their small size, distinctive form, and high surface-to-volume ratio (Khan *et al*., 2019; Ahmed *et al*., 2024; Eid 2025); the use of iron oxide nanoparticles raises major concerns regarding possible hazards to human health and the environment (Kurapov *et al*., 2019; Rana 2020; Siddiqui *et al*., 2023; Ahmed *et al*., 2024; Singh *et al*., 2025). Besides numerous advantages, little is known hemato-hepatotoxic impact of iron nanoparticles and aggravate becomes the situation when there are no established techniques available for

assessing their effects. Thus, this knowledge gap makes it imperative to focus on the assessment of toxicity of IONPs to warrant the safety of both humans and the environment (Siddiqui *et al*., 2023; Ahmed *et al*., 2024; Muhammad *et al*., 2025; Singh *et al*., 2025). Therefore, the current study was conducted to assess the hepatotoxic and hematotoxic effects of iron oxide nanoparticles (IONPs) in Sprague-Dawley rat, a model vertebrate.

MATERIALS AND METHODS

Iron oxide Nanoparticle Preparation: Ferrous chloride ($FeCl_2$, 10 mL), ferric nitrate nonahydrate ($Fe(NO_3)_3 \cdot 9H_2O$, 20 mL), citric acid (44.44 mL), deionized/distilled water, ethanol and a 17M ammonia solution for pH correction were used for the preparation of nanoparticles following the sol-gel auto-combustion technique. Using a magnetic stirrer, stoichiometric quantities of citric acid, $FeCl_2$ and $Fe(NO_3)_3 \cdot 9H_2O$ were dissolved in deionized water and thoroughly mixed. Concentrated ammonia was added gradually to bring the mixture's pH down to 7.0. To create a xerogel, the solution was heated to 353-363 K while being constantly stirred. After around two hours, spontaneous auto-combustion took place as the gelation was complete, producing a fluffy and dry powder. To create a spinel phase with a face-centered cubic (fcc) structure, this powder was pulverized using a mortar and pestle and then annealed for six hours at 1173 K.

Experimental design

Animal procurement and housing: The 25 male Sprague-Dawley rats, weighing 95-118 grams were procured from the Animal House, Department of Physiology, Government College University Faisalabad, Pakistan. The animals were given feed and water *at-libidum* during one-week acclimatization period, and ambient temperature was maintained at 25°C ± 2°C; humidity 52% and a 12-hour light/dark cycle.

Animal grouping and treatment: Rats were randomly divided into five groups (n=5 per group) following acclimatization. Every day for 28 days in a row, the iron oxide nanoparticles were injected intraperitoneally. To take injection-induced stress into consideration, 9% saline was injected intraperitoneally into the saline group rats.

Sample collection: At the end of the exposure time, rats were anesthetized, and heart punctures were used to obtain blood for hematological and biochemical analyses. For histological examination, liver tissues were removed, cleaned with PBS, and preserved in 10% neutral buffered formalin.

Hematological analysis: For hematological analysis, blood samples were drawn and placed in tubes coated with EDTA. An automated hematology analyzer was used to measure the hemoglobin concentration, platelet count, red blood cell counts and white blood cell count. The obtained blood was centrifuged for 15 minutes at 4000 rpm to separate the serum. For upcoming biochemical tests, the supernatant (serum) was moved into Eppendorf tubes and kept at -20°C (Li *et al*., 2016).

Biochemical analysis: Using commercial diagnostic kits; serum liver enzyme activity, such as AST, ALT, lactate dehydrogenase (LDH) and alkaline phosphatase (ALP), were measured following the manufacturer's instructions (Li *et al*., 2016).

Histopathological analysis

Tissue Processing: For 48 hours, liver samples were preserved in 10% neutral buffered formalin. 100 mL of 37% formaldehyde was dissolved in 900 mL of distilled water along with 4 g of sodium phosphate monobasic (NaH_2PO_4) and 6.5 g of sodium phosphate dibasic anhydrous (Na_2HPO_4) to create the fixative (Li *et al*., 2016).

Dehydration and clearing: Following fixation, tissue samples were placed in tissue baskets with labels and dehydrated twice using a graded series of ethanol (30, 50, 70, 90 and 100%) for two hours each. Tissues were dehydrated and then immersed in xylene for one or two hours, respectively, to remove any remaining fluid (Li *et al*., 2016).

Embedding and sectioning: Melted paraffin wax was injected into cleared tissues for 45 and 60 minutes at 58°C and 69°C, respectively. After being placed in paraffin blocks, tissues were left to harden. A rotary microtome was used to cut thin slices (2-3 µm). Glycerin-albumin adhesive was applied to glass slides and ribbons were floated onto them before being dried at 37°C for the entire night (Li *et al*., 2016).

Staining procedure: The paraffin sections were rehydrated using decreasing grades of ethanol (100, 90, 70, 50, and 30%) after being dewaxed in xylene (three changes, two minutes each). Sections were counterstained with 1% eosin for 15 to 2 minutes after being stained with hematoxylin for 2 to 5 minutes and washed under running water. Slides were stained, cleaned, oven-dried and then mounted with Canada balsam (Li *et al*., 2016).

Microscopic examination: A light microscope was used to view the stained slices at 40X and 100X magnifications. For histological analysis, representative photomicrographs were taken.

Statistical analysis: Minitab 17 statistical software was used to analyze the data. For each group (n=5), the results are shown as mean ± standard deviation (SD). The one-way analysis of variance (ANOVA) and Tukey's post hoc test were used to compare the groups. Statistical significance was defined as a p-value of less than 0.05.

RESULTS

Characterization of iron oxide nanoparticles (IONPs)

Scanning electron microscopy: The morphological properties of the produced iron oxide nanoparticles were thoroughly revealed by SEM analysis (Fig. 1). The nanoparticles showed a heterogeneous distribution with noticeable agglomeration and voids at lower magnifications (Fig. 1; C1-0), indicating possible differences in dispersion behavior within biological

systems. A porous, sheet-like structure (Fig. 1; C1-1) suggested a sizable surface area that might improve reactivity and adsorption. Layered, flaky structures were revealed by further magnification (Fig. 1; C1-2), which may have been caused by synthesis conditions or magnetic interactions. Strong aggregation and noticeable surface roughness were visible at the maximum magnification (Fig. 1; C1-3), which may have an impact on cellular absorption and toxicity.

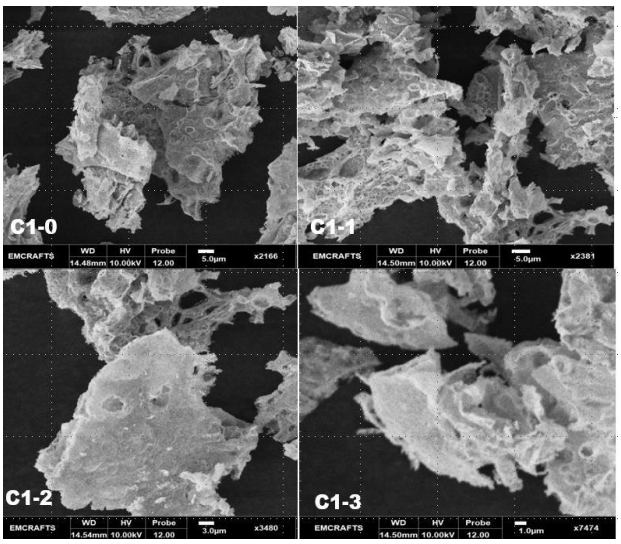

Fig. 1: SEM micrographs illustrating shape and aggregation behavior of iron oxide nanoparticles (IONPs)

X-ray diffraction (XRD) analysis: The crystalline character of the produced IONPs was validated by XRD examination (Fig. 2).The cubic spinel structure characteristic of Magnetite (Fe_3O_4) or maghemite (γ-Fe_2O_3) is represented by strong diffraction peaks seen between 2θ=30° and 70°, with a distinctively intense peak at 2θ=35°. The great purity of the produced nanoparticles was demonstrated by the lack of unnecessary peaks. In accordance with SEM measurements of particle size and shape, the average crystallite size was determined to be within the nanoscale range using the Scherrer equation (Kermanizadeh *et al*., 2013).

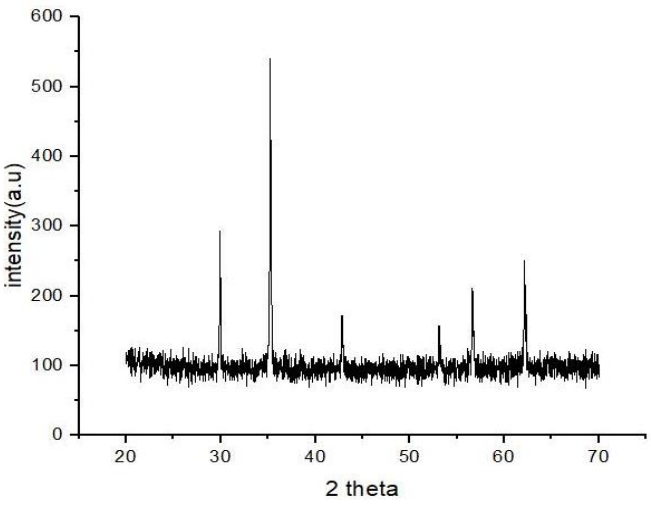

Fig. 2: The XRD pattern of synthetic iron oxide nanoparticles (IONPs) displays distinct, sharp peaks that validate the crystalline structure of the particles.

***In-vivo* studies**

General observations: Throughout the investigation, no deaths or serious clinical symptoms of toxicity were observed in any group. At first, little discomfort and dullness were observed, but later these went away on their own. No discernible abnormalities in movement, breathing, or behavior were found. Measurements of body weight showed a typical progressive increase in all groups, including those receiving different IONP dosages (Table 1).

Table 1: Weekly body weight (g) of Sprague-dawley rats exposed to different doses of Iron Oxide Nanoparticles and other groups

Weeks	Control group	Saline group 9%	Low dose group 75 mg/kg/day	Medium dose group 150 mg/kg/day	High dose group 300 mg/kg/day
Week 1	97.5±3.53	114.8±37.4	98.2±6.90	105.8±17.62	115.2±11.30
Week 2	122±2.82	121.6±16.05	129.4±10.6	135.4±27.33	136.8±11.8
Week 3	168.5±0.70	159.6±14.34	156.6±7.76	167.4±31.55	167.6±12.72
Week 4	180.5±2.12	169.6±14.34	176.4±9.34	189.2±34.75	187.6±17.70

Impact of IONPs formulation on liver function: Lipid profile analyses and liver function tests (LFTs; Table 2 & Fig. 3) showed dose-dependent changes in the experimental groups such as in Cholesterol, a substantial rise in the high-dose group's cholesterol (206±10 mg/dL) relative to the control group (142.7±10.97 mg/dL) suggested a disturbance in lipid homeostasis. As nanoparticle dosage increased, triglyceride levels rose as well, culminating at 167±19.97 mg/dL in the high-dose group, indicating a possible risk of metabolic disruptions. A consistent rise across groups, with the high-dose group achieving 464±24.27 mg/dL, further supported changes in lipid metabolism in Total lipids. HDL levels decreased from 50±3.61 mg/dL in controls to 34.33±3.79 mg/dL in the high-dose group, indicating a risk to the cardiovascular system. This inverse connection with dosage was clearly visible. Higher dosages cause LDL values to rise noticeably, indicating a poor cardiovascular profile. There was no discernible variation in bilirubin levels across groups, suggesting that hemolysis and bilirubin metabolism were not significantly affected. ALP levels significantly increased in the high-dose group (339.7±30.11 U/L) and medium-dose group (310±6.08 U/L), indicating biliary or hepatic stress. In Aspartate transaminase (AST/SGOT) and alanine transaminase (ALT/SGPT), both enzymes increased in response to dose, with the high-dose group having the highest levels (AST: 35.67±3.51 U/L; ALT: 49.33±4.04 U/L), which suggests hepatocellular injury.

Impact of IONPs on hematological parameters: Measuring hemoglobin concentration, total and differential white blood cell (WBC) counts, and platelet counts across various experimental groups (control, saline, low dose, medium dose, and high dose) allowed researchers to assess the hematological effects of iron oxide nanoparticles (IONPs) on Sprague-Dawley rats (Table 3 & Fig. 4).

The vital protein in red blood cells called hemoglobin oversees carrying oxygen throughout the body. Hemoglobin levels in all groups in this study stayed within the typical physiological range (12.1–15.1

g/dL for adult females and 13.8–17.2 g/dL for adult males). There were no statistically significant differences between the saline (16.5±0.46), low-dose (16.97±0.64), medium-dose (17±0.35), high-dose (17.6±1.57), and control (16.23±0.92) groups, suggesting that the administration of IONPs had no effect on hemoglobin concentration. An essential part of the immune response is played by white blood cells. WBC counts in the low-dose (6633±503.3/µL), saline (7300±916.5/µL), and control (7500±854.4/µL) groups were all within the typical reference range (4,500–11,000/µL) and did not differ substantially from one \another. The WBC counts of the medium-dose (10167±461.9/µL) and high-dose (11733±1305.1/µL) groups, however, exceeded the typical upper limit and showed a noteworthy and statistically significant dose-dependent rise. This suggests a possible inflammatory reaction or immunological activation brought on by increased IONP concentrations.

For hemostasis to be maintained, platelets are essential. Although there were minor changes, platelet counts in all groups stayed within the normal physiological range of 150,000–450,000/µL. While the saline (522000±22650/µL), low-dose (582000±28827/µL), and high-dose (611667±5033/µL) groups displayed slight variations without appreciable departure from normalcy, the control (631667±30072/µL) and medium-dose (632333±61199/µL) groups maintained the highest counts. The groups' neutrophil percentages varied from 51.33% to

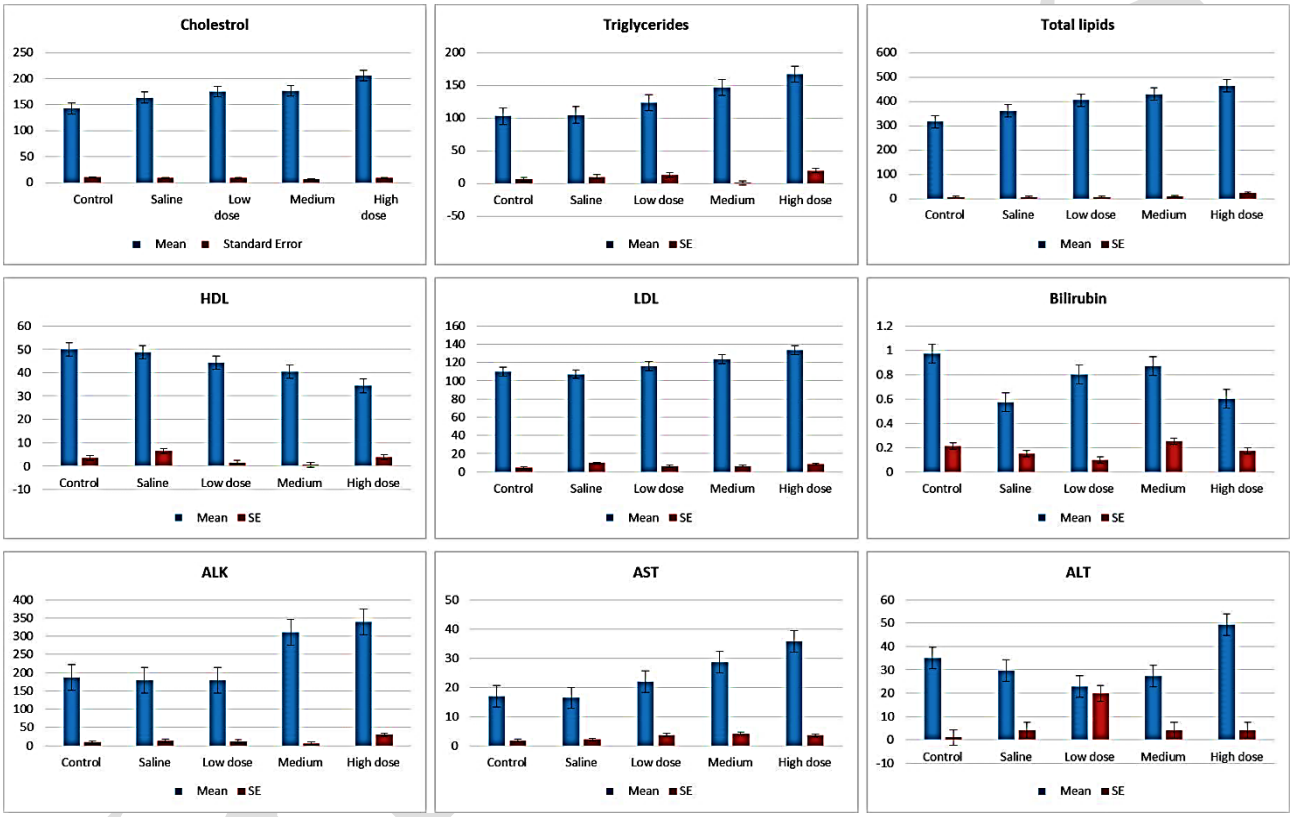

Fig. 3: Liver function and lipid profile markers in Sprague-dawley rats exposed to different doses of iron oxide nanoparticle.

Table 2: Liver function tests and lipid profile in Sprague-dawley rats exposed to different doses of iron oxide nanoparticle

	Control	Saline	Low dose	Medium	High dose
Cholesterol	142.7±10.97^{C}	163.7±9.07^{BC}	175±9.54^{B}	177±6.93^{B}	206±10^{A}
Triglycerides	103±6.56^{C}	105±10.15^{C}	124±13.11^{BC}	146.7±0.58^{AB}	167±19.97^{A}
Total lipids	317±6.24^{D}	360.7±5.03^{C}	405.7±5.51^{B}	430±10^{B}	464±24.27^{A}
HDL	50±3.61^{A}	48.67±6.43^{A}	44.33±1.53^{AB}	40.33±0.58^{AB}	34.33±3.79^{B}
LDL	109.7±4.62^{B}	107±9.54^{B}	116±6.24^{AB}	123.7±6.35^{AB}	133.3±8.74^{A}
Bilirubin total	0.97±0.21^{A}	0.57±0.15^{A}	0.8±0.1^{A}	0.87±0.25^{A}	0.6±0.17^{A}
ALK phosphate	187±8.89^{B}	178.7±13.65^{B}	179±11.53^{B}	310±6.08^{A}	339.7±30.11^{A}
ALT/ SGPT	35±1^{AB}	29.67±4.04^{AB}	22.83±19.98^{B}	27.33±4.16^{AB}	49.33±4.04^{A}
AST/ SGOT	17±1.73^{C}	16.33±2.08^{C}	22±3.61^{BC}	28.67±4.16^{AB}	35.67±3.51^{A}

P<0.05= Significant; same letters= non-significant.

Table 3: Hematological Markers in Sprague-dawley rats exposed to different doses of Iron Oxide Nanoparticles

	Control	Saline	Low dose	Medium	High dose
Hemoglobin	16.23±0.9238^{A}	16.5±0.4583^{A}	16.97±0.6429^{A}	17±0.3464^{A}	17.6±1.5716^{A}
WBCs	7500±854.4^{B}	7300±916.5^{B}	6633±503.3^{B}	10167±461.9^{A}	11733±1305.1^{A}
Platelets	631667±30072^{A}	522000±22650^{B}	582000±28827^{AB}	632333±61199^{A}	611667±5033^{AB}
Neutrophils	51.33±30.66^{A}	65±13.75^{A}	67.67±10.79^{A}	51.67±14.43^{A}	54±16.52^{A}
Lymphocytes	45.33±32.33^{A}	30±10^{A}	25.33±8.08^{A}	40±17.32^{A}	41.33±16.17^{A}
Monocytes	2±1^{A}	3.333±3.215^{A}	4.333±2.082^{A}	5±1.732^{A}	3±1^{A}
Eosinophils	1.333±1.155^{A}	1.667±1.155^{A}	2.667±1.155^{A}	3.333±1.155^{A}	1.667±0.577^{A}

P<0.05= Significant; same letters= non-significant.

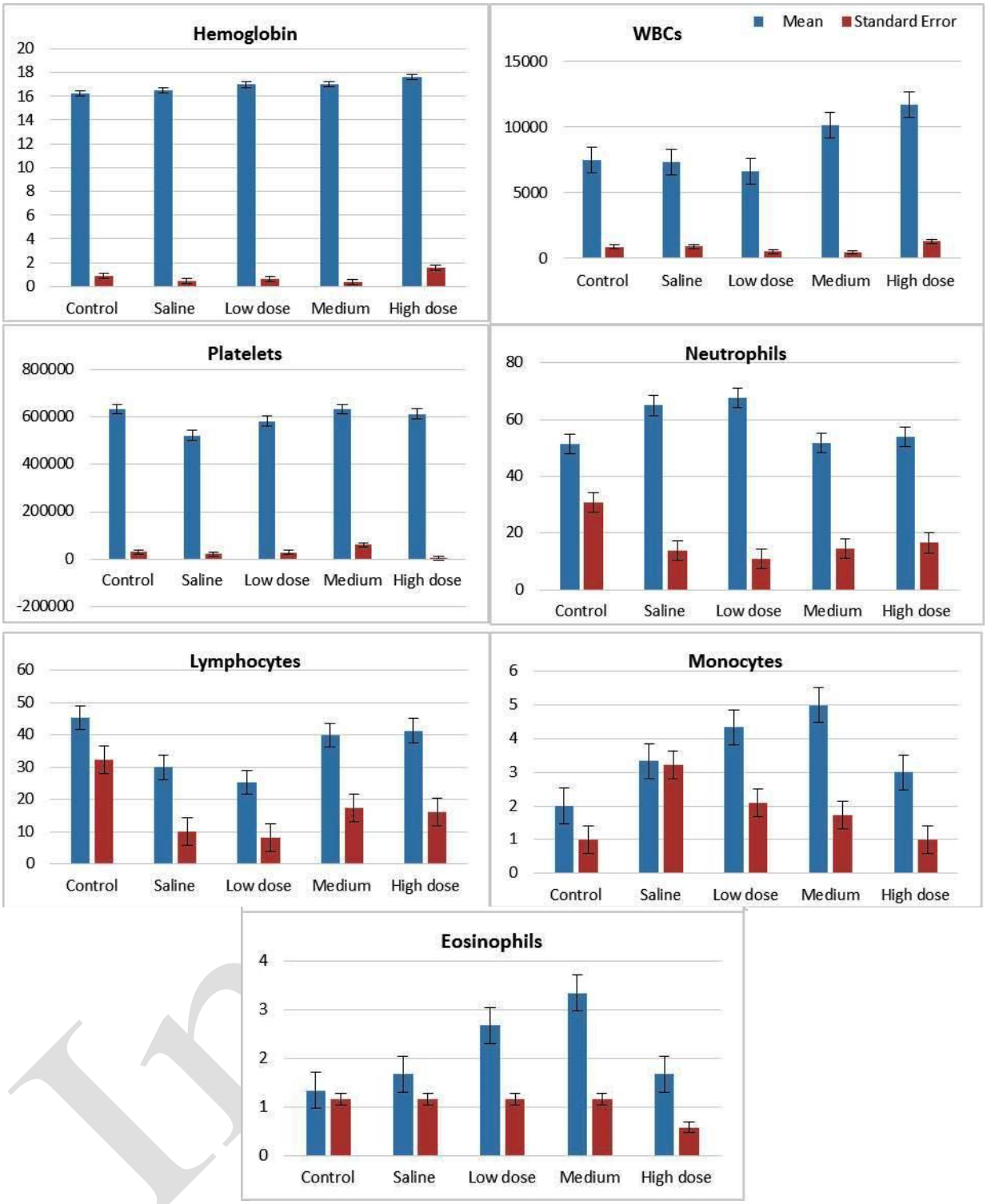

Fig. 4: Hematological parameters in Sprague-dawley rats exposed to different doses of iron oxide nanoparticle.

67.67% in relation to the differential WBC counts, which is in line with the usual reference range of 40–60%. There were no discernible differences between the groups, suggesting that IONPs had little effect on neutrophil response. Similarly, all groups' lymphocyte percentages were within the normal range (20–40%), ranging between 25.33% and 45.33% without showing any statistically significant changes. With only slight variations that were not statistically significant, monocyte percentages (2–8% reference range) stayed constant between groups. Eosinophil counts which normally make up 1 to 4% of the WBC population, stayed within normal ranges and did not significantly alter in response to treatment.

Together, these results imply that although greater dosages of IONPs can cause an increase in overall WBC counts, which is a sign of a systemic immunological response, their effects on platelet counts, red blood cells, and WBC differentials are comparatively minor. Overall, highly significant differences ($P<0.01$) were observed in cholesterol, triglycerides, total lipids, HDL, LDL, Bilrubin, ALT/SGPT, AST/SGOT concentration among different groups of Sprague-dawley rats (Table 2).

Moreover, there was a non-significant difference (P>0.05) in hemoglobin values, neutrophils, lymphocytes, monocytes and eosinophil counts, while a highly significant difference (P<0.01) was observed among the treated groups of albino rats (Table 3).

Histopathology of liver: A photomicrograph image of Sprague-dawley rat liver in Control group (A), Saline group (B), Low dose group (C), Medium dose group (D) and High dose group (E) represents the histological history of Liver. The image is H&E stain observed under 10X and 40X (Fig. 5).

Control group is a non-treatment group which displays the liver lobule's typical histological architecture, with all its key features present and in a well-organized state. The portal triad (PV, HA, and BD) is easily discernible, and hepatocytes radiate from the central vein. CV (Central Vein) is the primary vessel in the middle of the hepatic lobule. PV (Portal Vein) is a large channel that transports blood enriched with nutrients from the digestive system to the liver. Hepatic Artery (HA) provides the liver with blood that is rich in oxygen. Bile Duct (BD) transports hepatocyte-produced bile to the intestine and gallbladder. Kupffer cells, or KCs, are sinusoidal-dwelling liver macrophages that carry out phagocytosis. S (Sinusoids) are capillary-like structures that provide blood exchange between hepatocyte plates (Fig. 5A).

Saline group is a non-treatment group which received normal saline (Fig. 5B). This group demonstrates vascular congestion in the portal vein branch, where erythrocyte buildup causes the artery and surrounding sinusoids to dilate. This pathological alteration suggests decreased blood flow, which could be brought on by the toxicity of nanoparticles. PV (Portal Vein) was giving the appearance of a huge ship. Vascular Congestion (VC) is an abnormal buildup of blood in the blood vessel, it causes dilatation. SD (Sinusoids) is Hepatocyte-to-hepatocyte spaces, which are probably dilated because of congestion. EB (Erythrocytes in Blood), inside the clogged channel, red blood cells are evident.

Low dose group received 75mg/kg of chemically produced iron oxide nanoparticles intraperitoneally for 28 days (Fig. 5C) and depicts excess iron in the liver, as demonstrated by hemosiderin deposits. The presence of hemosiderin, a storage form of iron, suggests iron buildup, which may be brought on by exposure to iron oxide nanoparticles. Periportal edema is indicative of tissue swelling and inflammation. The swelling surrounding the portal area is known as periportal edema, or PE. Hemosiderin (ID) is a brownish-orange pigment that shows hepatocytes or macrophages have accumulated iron. While, Hepatocytes (HB), Kupffer cells (KC) and sinusoids (SD) are the cell surrounding the liver tissue.

Medium dose group received 150 mg/kg of chemically produced iron oxide nanoparticles intravenously for 28 days (Fig. 5D) and shows extreme congestion in the central vein, with red blood cells packed inside. This raises the possibility of liver damage and reduced venous outflow. There are Kupffer cells, which can become active in reaction to damage. Central Vein (CV) is the big vessel in the middle. In Vascular Congestion (VC), Erythrocytes are crammed into the major vein. Hepatocytes (HB), Kupffer cells (KC) and sinusoids (SD) are the cells that surround the liver and sinusoids.

High dose group received 300 mg/kg of chemically produced iron oxide nanoparticles intravenously for 28

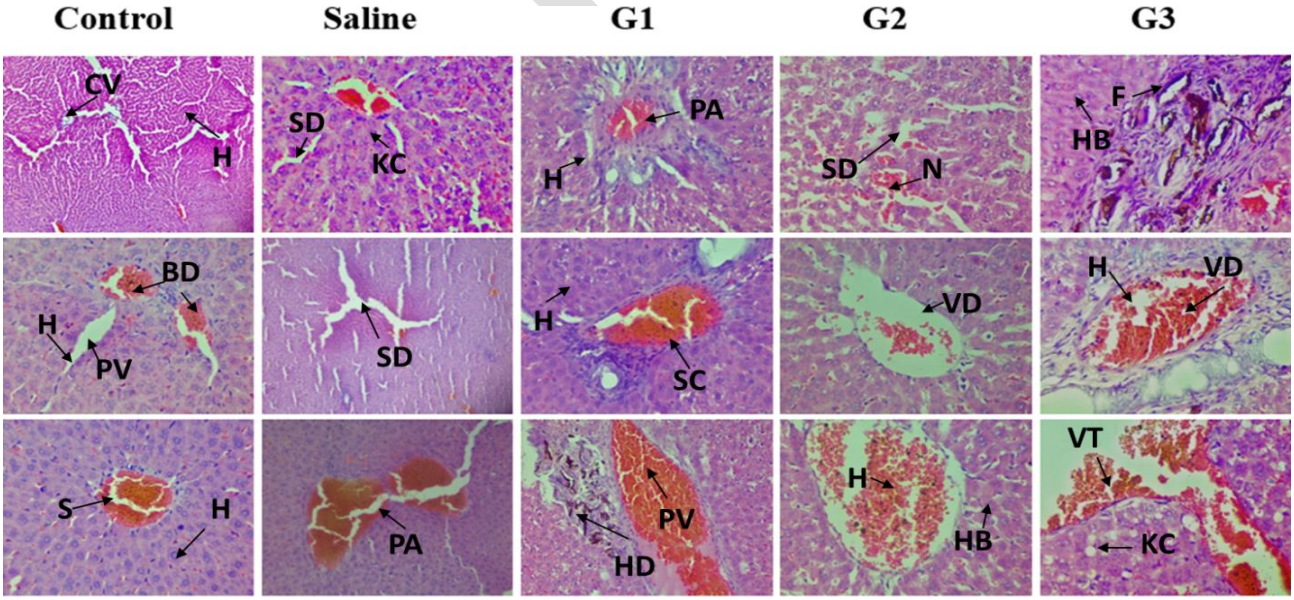

Fig. 5: Photomicrograph of Sprague-dawley rat liver in Control, Saline, Group 1 (Low dose group), Group 2 (Medium dose group) and Group 3 (High dose group E). The image is H&E stain observed under 40X. Histological examination of liver tissues stained with H&E reveals a progressive pattern of hepatic damage across the experimental groups. The Control group shows normal liver architecture with intact central veins (CV), portal vein (PV), bile duct (BD), sinusoid (S) and hepatocytes (H). The Saline group remains largely normal, with only mild sinusoidal dilation (SD), portal inflammation (PI) and kupffer cells activation (KC). In Group 1 (G1), early signs of liver injury appear, including portal area inflammation (PI), moderate sinusoidal congestion (SC) and hepatocyte degeneration (HD). Group 2 (G2) exhibits severe damage, with evident hepatocytes necrosis (N), vascular damage (VD), hemorrhage (H), hepatocytes ballooning (HB) and inflammatory infiltration. The extensive hemorrhage and damages are seen in Group 3 (G3), where marked fibrosis (F), vessels dilation (VD) and vessel thrombosis (VT) which is vascular congestion and disorganized hepatic structure indicate advanced liver injury. These findings suggest a dose-dependent hepatotoxic effect likely induced by the experimental compound.

days (Fig. 5E) displays inflammation (portal hepatitis), vascular congestion and fibrotic alterations (scarring) surrounding the portal vein. Chronic liver damage is indicated by fibrosis, which may be brought on by extended exposure to harmful nanoparticles. The portal vein, or PV, is a large vessel located in the portal tract. Vascular congestion, or VC, is the buildup of blood within the portal vein. CT (F) (Connective Tissue Fibrosis) is Fibrous tissue around the portal region that suggests fibrosis or scarring. Portal hepatitis, or PH, is characterized by inflammatory alterations in the portal tract. Hepatocytes (HB) and sinusoids (SD) are cells that surround the liver. All these images are observed under 10X and 40X.

DISCUSSION

Iron oxide nanoparticles are widely used in medical and biological applications worldwide. Although, because of their large surface area and nanoscale size, iron oxide nanoparticles (IONPs) tend to aggregate which causes surface instability; however, their magnetic and functional qualities are diminished by this instability, which are frequently modified through polyvinyl alcohol and polyethylene glycol (PEG), the polymers to increase their stability and biomedical applicability (Parivar *et al*., 2016). But the concerns about their possible toxicity, bioaccumulation, and environmental impact nevertheless exist despite their promising applications (Siddiqui *et al*., 2023; Ahmed *et al*., 2024; Muhammad *et al*., 2025; Singh *et al*., 2025). Male Sprague-dawley rats were used in this study to assess how IONPs affect their lipid metabolism, liver function, and immune system. High dosages of α-Fe_3O_4nanoparticles caused acute poisoning symptoms which included tremors, fast breathing, and lethargy (Abawy *et al*., 2023), which is in line with earlier work (Gaharwar *et al*., 2019). Histological analyses showed dose-dependent liver damage, with severe hepatic necrosis, fibrosis, and inflammation at higher concentrations and modest sinusoidal dilatation and Kupffer cell activation at lower dosages. The buildup and metabolic activity of IONPs within hepatic tissues are probably connected to these clinical alterations, which signify compromised liver function. By reabsorbing IONPs, Kupffer cells seem to play a crucial part in causing cellular damage and the production of harmful byproducts. This is consistent with earlier observations of hepatic bleeding, inflammatory infiltration, and hemosiderin deposits in rats treated with IONP (Kamel & AL-Taee, 2020). Similarly, the current findings agree to Aboulhoda *et al*. (2023) who shed light on IONPs' possible hepatotoxicity and hematotoxicity. They revealed that acute exposure to α-FeO (γ- Fe_2O_3) nanoparticles in rats results in symptoms such as subcutaneous bleeding, fast breathing, and lethargy. One of the main toxic mechanisms that has been revealed is oxidative stress. Reduced antioxidant enzymes glutathione (GSH), catalase (CAT), and superoxide dismutase (SOD) and elevated malondialdehyde (MDA) levels imply that IONPs encourage lipid peroxidation and interfere with antioxidant defense systems, resulting in membrane damage and cell death. In contrast to other metal oxide nanoparticles, no DNA damage was apparent despite the presence of oxidative stress; perhaps because the modest amount of ROS was insufficient to break DNA strands (Aboulhoda *et al*., 2023; Hasabo *et al*., 2024). Lipid metabolism changes were also noticeable. Total lipids, triglycerides, and cholesterol were markedly elevated by IONP exposure, especially at higher dosages, suggesting a disturbance in lipid homeostasis. Concerns regarding cardiovascular risks were raised by changes in HDL and LDL values, which indicated an atherogenic lipid profile. At the same time, hepatotoxicity and bile duct dysfunction were supported by markedly increased dose-dependent values of liver enzymes (ALT, AST, and ALP). Histopathological evidence of liver congestion and necrosis agreed with these analytical results (Awaad *et al*., 2024). At medium and high doses, hematological examination revealed increased white blood cell counts, which likely indicated systemic immunological activation brought on by oxidative stress. However, the levels of neutrophils and lymphocytes did not alter, suggesting that the immune system was activated generally without any changes in cell type. High-dose exposure resulted in a decrease in RBC count, probably because of oxidative damage and reduced erythropoiesis, whereas hemoglobin and platelet levels stayed constant. This is in line with earlier findings that linked exposure to nanoparticles to anemia-like effects (Aboulhoda *et al*., 2023).

The current findings overall highlight the hepatotoxic and hematotoxic effects of IONPs in Sprague-Dawley rats in dose-dependent manner. Disrupted lipid metabolism, increased liver enzymes, and substantial histological damage show how vulnerable the liver is as the main detoxifying organ. These results highlight the necessity of further long-term research work to assess the effects of chronic exposure and then develop safety standards for the use of IONPs in biomedicine, medical and biological applications.

Conclusions: Iron oxide nanoparticles (IONPs) induced dose-dependent physiological and toxicological changes. Rats receiving treatment had less weight growth, which suggested metabolic disturbance and systemic stress. Hematological alterations that suggested anemia and inflammation included elevated WBCs, reduced hemoglobin, RBCs, and hematocrit. The biochemical results revealed dyslipidemia and increased liver enzymes (ALT, AST, and ALP). The progression of liver injury from modest edema to severe fibrosis was confirmed by histological investigation. Iron overload, oxidative stress, and inflammatory reactions were important mechanisms. At medium levels, vascular congestion and Kupffer cell activation were observed. Excessive dosages caused fibrosis, lobular disruption, and portal inflammation. Despite IONPs' potential for biomedicine, findings pose significant safety concerns. More research is needed to determine safer formulations, antioxidant methods, and long-term effects.

Author Contributions: MKZ and FJ designed and supervised the work; MA performed the experiments; SI helped nanoparticles preparation and SEM; MM helped in rearing and experimentation; HR helped for data analyses

and write-up. All the authors read and approved the final version of the manuscript.

Acknowledgments: The facilities and support provided by the Department of Zoology, Government College University Faisalabad; Department of Pharmacology, Government College University Faisalabad, Department of Physics, Government College University Faisalabad are highly acknowledged.

REFERENCES

Abawy NA and AL-zubaidy MH, 2023. Evaluating the toxic oral doses of iron oxide nanoparticles in mice. Iraqi J Vet Sci 37(4): 801-811.

Abd Elaliem NM, Abdeen AAH, Ibrahim SS, *et al*., 2023. Prospective ameliorative activity of neem (*Azadirachta indica*) on iron oxide nanoparticle-induced multiple organ injury via attenuating TNF-α pathway. Benha Vet Med J 44(1): 55-60.

Aboulhoda BE, Othman DA, Rashed LA, *et al*., 2023. Evaluating the hepatotoxic versus the nephrotoxic role of iron oxide nanoparticles: One step forward into the dose-dependent oxidative effects. Heliyon 9(11): 1-6.

Ahmed R, Khan MS and Ali M, 2024. Advances in nanoparticle-based technologies for biomedical and environmental applications. J Nanotech Res 26(2): 134-147.

Al Alalaq MA, Al–Hadedee LT and Alrubeii AMS, 2023. Effect of iron oxide nanoparticles prepared by chemical method on the kidneys, liver and brain of male mice. In *IOP* Conference Series: Earth and Environmental Science 1252(1): 012132.

ALRashdi BM, Germoush MO, Sani SS, *et al.,* 2023. Biosynthesis of *Salvia hispanica* Based Silver Nanoparticles and Evaluation of their Antibacterial Activity in-vitro and Rat Model. Pak Vet J 43(2): 283-289. http://pvj.com.pk/pdf-files/23-123.pdf.

Awaad A, Rushdy A, Adly MA and Abd-Elsamei WM, 2024. Comparative analysis of biochemical abnormalities induced by iron oxide nanoparticles in some organs of albino rat and domestic pigeon and the role of deferoxamine as iron chelator. Sohag J Sci 9(4): 583-590.

Benjamin AS and Nayak S, 2025. Iron oxide nanoparticles coated with bioactive materials: a viable theragnostic strategy to improve osteosarcoma treatment. Discover Nano 20(1): 1-22.

Bică G, Rogoveanu OC, Gherghina FL, *et al*., 2024. The Histological and Biochemical Assessment of Monoiodoacetate-Induced Knee Osteoarthritis in a Rat Model Treated with Salicylic Acid-Iron Oxide Nanoparticles. Biol 13(5): 331.

Buck AC, Maarman GJ, Dube A and Bardien S, 2025. Mitochondria targeted nanoparticles for the treatment of mitochondrial dysfunction-associated brain disorders. Frontiers Bioengineering Biotech 13: 1563701.

Dietrich J, Enke A, Wilharm N, *et al*., 2023. Energetic electron-assisted synthesis of tailored magnetite (Fe_3O_4) and maghemite (γ- Fe_2O_3) nanoparticles: structure and magnetic properties. Nanomaterials 13(5): 786.

Eid M, 2025. Future Perspectives of Multifunctional Magnetic Nanoparticles in Therapy, Biology, and Pharmacy. In: Multifunctional Magnetic Nanoparticles in Therapy, Biology, and Pharmacy. CRC Press, pp: 301-324.

Gaharwar US, Meena R and Rajamani P, 2019. Biodistribution, clearance and morphological alterations of intravenously administered iron oxide nanoparticles in male wistar rats. Int J Nanomed 9677-9692.

Hannan A, Du X, Maqbool B and Khan A, 2024. Nanoparticles as potent allies in combating antibiotic resistance: A Promising Frontier in Antimicrobial Therapy. Pak Vet J 44(4):957-967. http://dx.doi.org/10.29261/pakvetj/2024.227

Hasabo G, Elbasiouny M, AbdelSalam M, *et al*., 2015. Acute Hepatotoxicity of Nano-and Micro-sized Iron Particles in Adult Albino Rats; Histopathological changes. J Vet Pharma Sci Tech 4(2): 47-50.

Innuan P, Kongkarnka S, Thongtharb A, *et al*., 2025. Iron (III)–Quercetin Complex: In Vivo Acute Toxicity and Biodistribution of Novel MRI Agent. Int J Nanomed 20:1303-1320. https://doi.org/10.2147/IJN.S496015

Jasim RA, Luaibi NM and Ali MR, 2025. Effects of iron oxide nanoparticles on male rats' thyroid and kidney functions. J College Basic Edu 30(128): 37-51.

Joshi V and Awasthi R, 2025. Iron Homeostasis and Metabolism During Pregnancy: Exploring Innovative Drug Delivery Approaches for Treating Iron Deficiency Anemia in Pregnant Women. Archiv der Pharmazie 358(5): e12002.

Kamel HR and AL-Taee AA, 2020. Iron oxide nanoparticles induced histological alteration and fetal skeletal abnormalities in the embryo of Albino rats. Med.-Leg Update 20: 911-915.

Kazaryan SA, Oganian SA, Vardanyan GS, *et al*., 2024. Liver-targeting iron oxide nanoparticles and their complexes with plant extracts for biocompatibility. Beilstein J Nanotech 15(1): 1593-1602.

Kermanizadeh A, Balharry D, Wallin H, *et al* 2015. Nanomaterial translocation, the biokinetics, tissue accumulation, toxicity and fate of materials in secondary organs. a review. *Crit Rev Toxicol 45*(10): 837-872.

Khan I, Saeed K and Khan I, 2019. Nanoparticles: Properties, applications and toxicities. Arab J Chem 12(7): 908-931.

Kurapov YA, Vazhnichaya EM, Litvin SE, *et al*., 2019. Physical synthesis of iron oxide nanoparticles and their biological activity in vivo. SN Applied Sci 1: 1-11.

Laubertova L, Dvorakova M, Balis P, *et al*., 2022. Preliminary findings on the effect of ultrasmall superparamagnetic iron oxide nanoparticles and acute stress on selected markers of oxidative stress in normotensive and hypertensive rats. Antioxidants 11(4): 751. https://doi.org/10.3390/antiox11040751

Li Y, Wang J, Gao L, Tian Z, *et al*., 2016. Bioaccumulation and toxicity of carbon nanoparticles suspension injection in intravenously exposed mice. Int J Nanomed 11: 2737-2746.

Liu H, Zhen Z, Chen F, *et al*., 2025. Advancements in iron oxide nanoparticles for multimodal imaging and tumor theranostics. Current Med Chem 32(2): 301-321.

Ma Y, Wu H, Jia M, *et al.,* 2024. Construction of iron oxide nanoparticles modified with *Angelica sinensis* polysaccharide for the treatment of iron deficiency anemia. J Nanopart Res 26(11): 250. https://doi.org/10.1007/s11051-024-06169-y

Mirzajani F, Rostamzadeh A, Tahmasian Z, *et al*., 2024. Effects of MRI magnetic iron oxide nanoparticles on the structural and enzymatic properties of liver-related enzymes. Micro and Nano Syst Letters 12(1): 13-19.

Mohamed EK, Fathy MM, Sadek NA, *et al*., 2024. The effects of rutin coat on the biodistribution and toxicities of iron oxide nanoparticles in rats. J Nanopart Res 26(3): 49. https://doi.org/10.1007/s11051-024-05949-w

Muhammad S, Khan AA, Khan MR, *et al.,* 2025. Effective substitution of ferrous sulfate with iron oxide nanoparticles enhances growth, antioxidant activity, and stevioside accumulation in micro-propagated *Stevia rebaudiana*. Frontiers Plant Sci 16: 1569613.

Panda J and Das D, 2025. Superparamagnetic iron oxide nanoparticle-based nanosystems for cancer theranostics. Global Transl Med 4(2): 31-50.

Parivar K, Fard FM, Bayat M, *et al*., 2016. Evaluation of iron oxide nanoparticles toxicity on liver cells of BALB/c rats. Iran Red Cres Med J 18(1): 15-21.

Poonia N, Kumar V, Subudhi RN, *et al*., 2025. Iron oxide nanoparticles: a versatile nanoplatform for the treatment and diagnosis of ovarian cancer. Therapeutic Delivery 16(4): 379-392.

Rana SVS, 2020. A comprehensive assessment of hepatotoxicity induced by engineered nanoparticles a review. J Toxicol Risk Assessment 6(35): 115-126.

Rathore P, Verma S and Singh R, 2023. Nanomaterials in targeted drug delivery: Recent progress and future prospects. *J Cont Release 357*: 112-126.

Reddy UA, Prabhakar PV and Mahboob M, 2017. Biomarkers of oxidative stress for in vivo assessment of toxicological effects of iron oxide nanoparticles. Saudi J Biolog Sci 24(6): 1172-1180.

Regan CR, Sarangi S and Aranganathan V, 2025. Long-Term Toxicity of Silica-Coated Iron Oxide Nanocrystalline Clusters Used for Magnetic Hyperthermia Applications. BioNanoScience 15(1): 1-15.

Shah A, Sun H, Qiao Z, *et al*., 2024. Synthesis of Iron Oxide Nanoparticles and its Antimicrobial, Anticancer, Anti-inflammatory, Wound Healing, and Immunomodulatory Activities-A Review. Phytopharm Res J 3(3): 1-28.

Shokrollahi F, Salehzadeh A, Kafilzadeh F and Zaefizadeh M, 2023. Evaluation of the effect of iron oxide nanoparticles functionalized by glucose and conjugated with coumarin (Fe3O4@ Glu-Coumarin NPs) on the expression of CASP8, CASP9, p53, mTOR1, and MAPK1 genes in liver cancer cell line. Gene Reports 33: 101818.

Siddiqui MA, Wahab R, Saquib Q, *et al*., 2023. Iron oxide nanoparticles induced cytotoxicity, oxidative stress, cell cycle arrest, and DNA damage in human umbilical vein endothelial cells. J Trace Elements Med Biol 80: 127302.

Singh P, Pandit S, Balusamy SR, *et al*., 2025. Advanced nanomaterials for cancer therapy: gold, silver, and iron oxide nanoparticles in oncological applications. Adv Healthcare Mater 14(4): 2403059.

Szymczuk D, Markiewicz KH, Niemirowicz-Laskowska K, *et al*., 2025. Covalent modification of iron oxide-poly (lithocholic acid) nanoparticles with folic acid or doxorubicin–an approach for enhanced cancer therapy. RSC Advances 15(18): 14246-14258.

Taher GN and Ghareeb OA, 2022. Adverse effects of iron oxide nanoparticles on some biochemical markers and ameliorative effect of Silymarin. Biochem Cellular Arch 22(1): 1829-1832.

Zhang C, Cha R, Long K, *et al.,* 2024. Functionalized Iron Oxide Nanoparticles for Both Dual-Modal Imaging and Erythropoiesis. ACS Applied Mater Interfaces16(50): 68905-68917.